On the Polarization of $H\alpha$ Scattered by Neutral Hydrogen in Active Galactic Nuclei

Hee-Won Lee and Jong-Hyeun Yun

Department of Astronomy, Seoul National University, Seoul, 151-742, Korea

Accepted 1998 July 28. Received 1998 July 27; in original form 1998 July 26

ABSTRACT

Raman scattering by atomic hydrogen converts the UV continuum around $\text{Ly}\beta$ into optical continuum around $\text{H}\alpha$, and the basic atomic physics has been discussed in several works on symbiotic stars. We propose that the same process may operate in active galactic nuclei (AGN) and calculate the linear polarization of the broad emission lines Raman-scattered by a high column neutral hydrogen compnent. The conversion efficiency of the Raman scattering process is discussed and the expected scattered flux is computed using the spectral energy distribution of an AGN given by a typical power law. The high column H I component in AGN is suggested by many observations encompassing radio through UV and X-ray ranges.

When the neutral hydrogen component with a column density $\sim 10^{22}$ cm⁻² is present around the active nucleus, it is found that the scattered H α is characterized by a very broad width $\sim 20,000$ km s⁻¹ and that the strength of the polarized flux is comparable to that of the electron-scattered flux expected from a conventional unified model of narrow line AGN. The width of the scattered flux is mainly determined by the column density of the neutral scatterers where the total scattering optical depth becomes of order unity. The asymmetry in the Raman scattering cross section around Ly β introduces red asymmetric polarized profiles around H α . The effects of the blended Ly β and O VI 1034 doublet are also investigated.

We briefly discuss the spectropolarimetric observations performed on the Seyfert galaxy IRAS 110548-1131 and the narrow line radio galaxy Cyg A. Several predictions regarding the scattering by a high column neutral hydrogen component in AGN are discussed.

Key words: polarization - scattering - - galaxies : active - galaxies : nuclei

1 INTRODUCTION

The spectra of active galactic nuclei (hereafter AGN) are characterized by many prominent emission lines. The width of the emission lines is one of the important parameters to classify these active galaxies. For example, type 1 Seyfert galaxies possess both broad and narrow emission lines and type 2 Seyfert galaxies exhibit only narrow emission lines (e.g. Osterbrock 1989). Radio galaxies are also classified into broad line radio galaxies and narrow line radio galaxies in a similar way. The width of the broad emission lines (BEL's) often ranges up to several thousand km s⁻¹ and the narrow emission lines (NEL's) show an order of magnitude smaller width in both type Seyfert galaxies.

A unification model of Seyfert galaxies suggests that Seyfert 2 nuclei also have the broad emission line region (BELR), which is blocked from the observer's line of sight. In this unification scheme, the BEL photons can be scattered from other lines of sight to enter the observer's line of sight. Because the scattered component is expected to be highly

polarized, spectropolarimetry plays an important role to test the unification models (e.g. Antonucci 1993).

A similar behavior is seen in broad absorption line quasars, in which the broad absorption trough is partially filled by photons scattered from other lines of sight. These photons are believed to be scattered resonantly by a fast moving medium just outside the BELR, and several spectropolarimetric observations using large telescopes such as the Keck 10 m telescope have been performed (e.g. Cohen et al. 1995, Goodrich & Miller 1995, Lee & Blandford 1997).

Spectropolarimetry of Seyfert 2 galaxies performed by several researchers confirmed that the BEL's are shown in the polarized flux as expected from the unification scheme (e.g. Antonucci & Miller 1985, Miller & Goodrich 1990, Antonucci 1993). The constant position angle and degree of polarization favor strongly the model, in which the electron plasma located in high latitude scatters the radiation originated from the BELR into the observer's line of sight.

Tran (1995 a,b,c) presented the spectropolarimetric data on a number of Seyfert 2 galaxies, which exhibit broad

emission lines in the polarized flux. He noted that the Balmer lines are more highly polarized than the adjacent continuum even after all the corrections due to the star light and the interstellar medium. He proposed an explanation by assuming that there is still unpolarized continuum having a flat spectra not included in the correction procedures. This component provides more dilution to the continuum leaving the lines more polarized. However, higher stellar contribution as suggested by Koski (1978) would result in wavelength independent polarization (Antonucci, 1993).

Another interesting and important spectropolarimetric observation is presented by Ogle et al. (1997), who observed the narrow line radio galaxy Cyg A. They found that the H α polarized flux has a very broad width exceeding 20000 km s⁻¹. Young et al. (1993) also found very broad polarized H α from their spectropolarimetry of the Seyfert 2 galaxy IRAS 110548-1131, where the full width at zero intensity is 16800 km s⁻¹.

The X-ray observations of Seyfert galaxies have been performed to elucidate the physical properties of the highly ionized component plausibly related with the scattering agents of the Seyfert 2 galaxies. The warm absorbers having a column density of $N_H \sim 10^{21}-10^{22}~{\rm cm}^{-2}$ are invoked to explain the soft X-ray observations of Seyfert galaxies. On the other hand, the existence of the neutral component with a similar column density is controversial (e.g. Marthur 1997).

Conway & Blanco (1995) used the VLA to obtain the H I column density $N_{H\,\rm I}\sim 10^{22-23}~{\rm cm}^{-2}$ toward the compact nucleus of Cyg A, by measuring the 21 cm absorption. The neutral hydrogen is concentrated near the nucleus within several parsecs and they suggested that atomic hydrogen is an important constituent of the molecular torus obscuring the BELR of the narrow line radio galaxy. Their result is compatible with an X-ray spectroscopy by the Ginga satellite (e.g. Ueno et al. 1994) suggesting a highly optically thick component around the compact nucleus.

Strongly polarized broad emission features around $\lambda\lambda6830$, 7088 in a fair fraction of symbiotic stars were recently identified to be Raman-scattered O VI $\lambda\lambda 1032$, 1038 by atomic hydrogen of large column density (e.g. Schmid 1989, Nussbaumer et al. 1989). The absorbed UV photons with wavelength $\lambda_i < \lambda_\alpha = 1216 \text{ Å by a hydrogen atom}$ in the ground state 1s can be re-emitted either coherently with wavelength $\lambda_f = \lambda_i$ (the Rayleigh scattering) or incoherently with $\lambda_f = (\lambda_i^{-1} - \lambda_\alpha^{-1})^{-1}$ (the Raman scattering). Therefore, UV continuum photons near Ly β are scattered and transformed into optical photons around $H\alpha$ by the Raman process. One of the most important characteristics of the Raman scattering process is the enhancement of the Doppler shift so that the scattered waves appear to be shifted by a factor of $\sim \lambda_f/\lambda_i$, and this leads to a formation of a very broad line feature from a moderately broad incident radiation source.

The Raman process can be important in the systems having both a strong UV incident radiation source and a neutral hydrogen component of large column density. The optimum conditions for the Raman scattering may be provided by AGNs, where the spectral energy distribution (SED) is characterized by the big blue bump in the UV range and neutral components with a high column density may be found near the broad line region. As in symbiotic stars, the

Raman scattering may produce observable features around $H\alpha$ both in the profile and in the polarization.

In this paper we investigate the possible observational features expected if the Raman process operate in AGN. The paper is composed as follows. In section 2, we give a model description and make an estimate of the strength of the Raman-scattered flux using a standard AGN model. In section 3, the Monte Carlo result is presented and compared with the electron-scattering model. We discuss the application of the Monte Carlo result to a couple of narrow line AGN and the observational implications in section 4. We summarize in the final section.

2 MODEL

2.1 Scattering by a high column neutral hydrogen

The polarized fluxes of many Seyfert 2 galaxies are characterized by a constant position angle and a constant degree of polarization, which strongly indicate that they have the electron scattering origin. The width of the broad polarized flux puts a constraint on the electron temperature $T_e \lesssim 10^5$ K. Assuming a covering factor $\gtrsim 0.1$ and a similar luminosity of the hidden broad line region of Seyfert 2 galaxies to that of Seyfert 1 galaxies, one can deduce that the electron column density is of order 10^{22} cm⁻² (e.g. Miller & Goodrich 90).

Recent X-ray observations on several Seyfert galaxies have shown that there exists a highly ionized component of column density $10^{21}-10^{22}~{\rm cm}^{-2}$. The warm absorber model has been introduced to account for the X-ray absorption as well as the UV absorption properties of the Seyfert galaxies (e.g. Marthur 1997, Kriss et al. 1995). Therefore the warm absorber may provide a good candidate for the free electron scatterers of the UV photons originating from the broad line region.

A high column neutral component has been suggested from X-ray observations of Seyfert galaxies (Turner et al. 1996, Nandra et al. 1994, Netzer 1993). The physical nature of the X-ray absorbing material in AGN is still controversial, and the possibility that both cold and warm absorbers may co-exist is not excluded.

Many X-ray observations of Seyfert 2 galaxies show that Compton reflected components seen in the spectra in the band 0.1 keV - 10 keV are compatible with the assumption of the molecular torus supplying the cold optically thick material. It is not certain whether the neutral absorbers suggested for the X-ray observations of Seyfert 1 galaxies are also originated from the molecular torus or constitute an independent component in the center part of AGN.

More direct information about the amount of neutral hydrogen can be obtained from radio observations using the 21 cm line from the hyperfine structure of hydrogen atom. Dickey (1986) investigated the content of neutral hydrogen in 19 active spiral galaxies and obtained values in the range $N_{H\,I}\sim 10^{20-22}(T_s/100~{\rm K})~{\rm cm}^{-2}$. He also mentioned the possibility that the spin temperature T_s may reside in a large range 10^{2-4} K, in which case a column density as high as $10^{23}~{\rm cm}^{-2}$ is also allowed.

Similar observations have been made by a number of researchers including Gallimore et al. (1994), Mundell et al. (1995). It seems that the results of these observations produce more or less similar values for the neutral column

density around the galactic nuclei.

In this subsection, we investigate the scattering properties of atomic hydrogen. We will assume a neutral component along the normal direction to the accretion disk with a covering factor of about 0.1 and column densities 10^{21-23} cm⁻².

Interactions of electromagnetic waves with atoms are described by the Kramers-Heisenberg formula (e.g. Sakurai 1967). The scattering types are divided into the Rayleigh scattering and the Raman scattering, where in the former case the initial and the final states of the scatterer are the same and the scattering is coherent. On the other hand, in the case of the Raman scattering the final state of the scatterer differs from the initial state and therefore the scattered photon has different frequency from that of the incident one. The explicit numerical computation of the relevant scattering cross sections has been done by many researchers (Gavrila 1967, Saslow and Mills 1969, Schmid 1989, Isliker et al. 1989, Sadeghpour & Dalgarno 1992, Lee & Lee 1997a).

Following Lee & Lee (1997a), the Rayleigh and the Raman scattering cross sections are given by

$$\frac{d\sigma_v}{d\Omega} = r_0^2 \left(\frac{\omega'}{\omega}\right) \times \left| (\epsilon \cdot \epsilon') \left(\sum_n M_v^b(n) + \int_0^\infty dn' M_v^c(n') \right) \right|^2,$$
(2.1)

where the subscript $v=\{Ray,\ Ram\}$ represents the scattering type, $r_0=\frac{e^2}{m_ec^2}$ is the classical electron radius, ω and ϵ are the angular frequency and the polarization vector for the incident wave and the primed quantities correspond to the scattered wave. The matrix elements for the bound states are

$$M_{Ray}^{b}(n) = \frac{1}{3} \frac{m_e \omega \omega'}{\hbar} < 1s \parallel r \parallel np > < np \parallel r \parallel 1s >$$

$$\times \left(\frac{1}{\omega_{r1} - \omega} + \frac{1}{\omega_{r1} + \omega'} \right),$$

$$(2.2)$$

and

$$M_{Ram}^{b}(n) = \frac{1}{3} \frac{m_{e} \omega \omega'}{\hbar} < 2s \parallel r \parallel np > < np \parallel r \parallel 1s >$$

$$\times \left(\frac{1}{\omega_{n1} - \omega} + \frac{1}{\omega_{n1} + \omega'} \right),$$
(2.3)

where the double-bar (or reduced) matrix elements for the position operator are found in Berestetskii et al. (1972) (see also Bethe 1967). Here, $\omega_{ni}\{i=1,2\}$ is the transition angular frequency between the level n and 1s or 2s depending on i. The contributions to the matrix elements M_{Ray}^c , M_{Ram}^c from the continuum states are similarly given (e.g. Saslow & Mills 1969).

In Fig. 1, we show the total (Rayleigh+Raman) and the Raman scattering optical depths for a neutral hydrogen slab of column density $N_{H\,\rm I}=10^{22}~{\rm cm}^{-2}$ as a function of the incident wavelength. We present the incident wavelength λ_i by the velocity deviation defined by $\Delta V=c(\lambda_i-\lambda_\beta)/\lambda_\beta$. A close inspection reveals that the total scattering cross section is also slightly asymmetric. More quantitatively, in the range $-850~{\rm km~s}^{-1}<\Delta V<1200~{\rm km~s}^{-1}$, the total scattering optical depth exceeds unity.

The ratio of the Raman scattering cross section to that of the total scattering cross section is also plotted in Fig. 1.

It is particularly notable that the ratio is asymmetrical. The ratio increases from 0.03 to 0.3 in the wavelength interval 1010 Å $<\lambda<$ 1040 Å. This implies that the conversion efficiency from UV around Ly β to optical around H α is much larger in the red part than in the blue part.

From Fig. 1, we see that for a slab of column $N_{H\,\rm I}=10^{23}~{\rm cm}^{-2}$ incident photons with the velocity difference satisfying $-3300~{\rm km~s}^{-1}<\Delta V<3100~{\rm km~s}^{-1}$ (or $1014~{\rm \AA}<\lambda<1036~{\rm \AA}$) have total scattering optical depth $\tau_{tot}>1$. The wavelength range considered in this work is described by the Lorentzian wing part, and the Doppler shift corresponding to the total scattering optical depth of unity depends approximately on the square root of the column density, i.e.,

$$|\Delta V| \sim 2000 \ N_{22}^{1/2} \ \text{km s}^{-1},$$
 (2.4)

where $N_{22} = N_{H \text{ I}}/(10^{22} \text{ cm}^{-2})$.

The incoherent nature of the Raman scattering process introduces an enhancement of the Doppler shift by the relation

$$\frac{\Delta \lambda_f}{\lambda_f} = \left(\frac{\lambda_f}{\lambda_i}\right) \cdot \left(\frac{\Delta \lambda_i}{\lambda_i}\right),\tag{2.5}$$

(e.g. Schmid 1989). In the case of incident photons having wavelengths similar to that of Ly β , the wavelength ratio $\lambda_f/\lambda_i \sim 6.4$, and therefore the incident photons having a width $\sim 2000~{\rm km~s^{-1}}$ around Ly β will result in a broad feature around H α with a width $\sim 13,000~{\rm km~s^{-1}}$. This implies that a broad line-like scattered feature with $\Delta V \gtrsim 15,000~{\rm km~s^{-1}}$ can be formed from a neutral hydrogen component with $N_{H\,\rm I} \gtrsim 10^{22}~{\rm cm^{-2}}$.

In this work, we do not consider the contribution of the H α line photons scattered by hydrogen atoms in excited states n=2, because the velocity width for this process to be important is a few times the thermal velocity width depending on the population of the excited state hydrogen atoms and is much smaller than the typical velocity scale of the BELR. Therefore, this process has a very small band width compared with that of the Raman scattering process. However, if we have a neutral scattering component covering a large velocity space ranging $\gtrsim 1000~{\rm km~s^{-1}}$, then this process should not be neglected.

2.2 Spectral Energy Distribution

In order to assess the flux Raman-scattered by neutral hydrogen and compare it with the flux scattered by free electrons, it is essential to know the SED of the AGN both in UV and in optical ranges. A typical AGN spectrum is characterized by the so called big blue bump in the ultraviolet range and the specific luminosity shows a peak at $\sim 10^{15}$ Hz (e.g. Mathews & Ferland 1987). It is conventional to represent the SED as a power law with the power index α so that we have

$$L_{\nu} = L_{\nu_0} \left(\frac{\nu}{\nu_0}\right)^{\alpha}. \tag{2.6}$$

Zheng et al. (1997) investigated more than 200 quasar spectra obtained from the Hubble Space Telescope (HST) and constructed composite quasar spectra. They concluded that the power law index $\alpha = -0.99 \pm 0.05$ in the continuum between 1050 Å and 2200 Å.

Natali et al. (1998) also investigated the optical-UV continuum SED using the spectra of 62 QSOs emphasizing

Figure 1.

Total (Rayleigh+Raman) and Raman scattering optical depths for a neutral hydrogen slab of column density $N_{H\,I}=10^{22}$ cm⁻². The horizontal axis shows the incident photon wavelength in units of Å. The solid line shows the total scattering optical depth and the Raman scattering optical depth is represented by the dotted line. The dashed line represent the ratio of the Raman scattering cross section to that of the total scattering cross section. The points marked by a cross are the velocity shifts having the total scattering optical depth of unity for $N_{H\,I}=10^{22}$ cm⁻², and the points marked by a circle are for $N_{H\,I}=10^{23}$ cm⁻².

that the local nature of the power-law approximation. They obtained the mean values of the power-law index change from $\alpha \sim 0.15$ at $\lambda > 3000$ Å to $\alpha \sim -0.65$ at $\lambda < 3000$ Å.

We assume that the incident spectrum in the UV and the optical ranges is given by a double power law, i.e.,

$$L_{\nu} = \begin{cases} L_{\nu_0} \left(\frac{\nu}{\nu_0}\right)^{\alpha_1} & \text{if } \nu > \nu_0 \\ L_{\nu_0} \left(\frac{\nu}{\nu_0}\right)^{\alpha_2} & \text{if } \nu < \nu_0, \end{cases}$$
 (2.7)

where $\nu_0 = 10^{15}$ Hz, and we set $\alpha_1 = -1$, and $\alpha_2 = 0.15$.

According to the prescription Eq. (2.7), the incident photon number flux Φ_{λ} is related with the specific luminosity

$$\Phi_{\lambda} \propto \lambda L_{\lambda} \propto \lambda^{-\alpha - 1},\tag{2.8}$$

and therefore, the continuum number flux near $H\alpha$ is given by

$$\Phi_{\lambda}(\lambda \sim \lambda_{H\alpha}) \sim 0.4 \times \Phi_{\lambda}(\lambda \sim \lambda_{L\beta}) \tag{2.9}$$

Lee & Lee (1997b) discussed the basic properties of the Raman scattering process, and gave an empirical formula of the efficiency ϵ_{Ram} for the conversion of the UV photons into the optical photons. They showed that the efficiency is quite large when the total scattering optical depth is moderately large, or, $\tau_{scat} \gtrsim 1$. Furthermore, the conversion efficiency is sensitively dependent on the ratio of the Raman scattering cross section to the total scattering cross section.

Using the relation

$$d\lambda_f = \left(\frac{\lambda_f}{\lambda_i}\right)^2 d\lambda_i. \tag{2.10}$$

and combining it with Eq. (2.9), we obtain the Raman-scattered continuum flux at around ${\rm H}\alpha$

$$\Phi_{\lambda}^{Ram} d\lambda_f \sim C_N \epsilon_{Ram} \Phi_{\lambda_i} d\lambda_i
\sim 0.06 \ C_N \epsilon_{Ram} \Phi_{\lambda_f} d\lambda_f.$$
(2.11)

Here, C_N is the covering factor of the neutral component having the total scattering optical depth $\gtrsim 1$, and $\lambda_f \sim 6563 \text{ Å}$, $\lambda_i \sim 1025 \text{ Å}$, respectively.

The continuum number flux Φ_{Th} that is Thomson scattered near H α depends on the electron column density and the covering factor. Hence, assuming that the scatterers have a small Thomson scattering optical depth $\tau_W < 1$, we may write

$$\Phi_{\lambda}^{Th} \sim C_W \tau_W \Phi_{\lambda_f}, \tag{2.12}$$

where C_W is the covering factor of the ionized scattering medium. Here, we ignore the line broadening by the thermal motions of the electrons.

Therefore, the Raman-scattered continuum flux around $H\alpha$ is compared with the Thomson-scattered continuum flux by the relation

$$\Phi_{\lambda}^{Ram} \sim \epsilon_{Ram} \left(\frac{\tau_W}{0.06}\right)^{-1} \left(\frac{C_N}{C_W}\right) \Phi_{\lambda}^{Th}.$$
 (2.13)

Under the assumption that the electron plasma has a column density $10^{22}~{\rm cm}^{-2}$ (or $\tau_W=0.6\times 10^{-2}$), and that the neutral hydrogen has the column of $N_{H\,\rm I}=10^{22}~{\rm cm}^{-2}$, the continuum flux that is Raman-scattered from Ly β with a width of 2000 km s⁻¹ is comparable to the Thomson-scattered at around H α with a width of 15,000 km s⁻¹.

Because ϵ_{Ram} is a sensitive function of the column density and the frequency, the Raman-scattering material can be regarded as a scattering-mirror with a narrow band width centered at the resonance frequencies (e.g. Lee & Lee 1997 a,b).

In an AGN spectrum, both Ly β and H α are very strong lines and especially Ly β is often blended with O vi 1034 to form a very broad feature around 1030 Å and thus the line photons are also an important constituent of the UV incident radiation (e.g. Laor et al. 1994, Laor et al. 1995, Netzer 1990).

2.3 Model and the Monte Carlo Method

We briefly describe the model and the Monte Carlo code to compute the polarization due to the neutral component. In this paper the neutral scatterers are placed along the symmetry axis for simplicity and ease of a direct comparison with electron-scattered flux. A more realistic model may be suggested by placing the neutral scatterers in the molecular torus, the top part of which is accessible by an observer with low latitude. If the molecular torus is approximated by a perfect cylinder with an inner radius a and a height h (e.g. Pier & Krolik 1992), then the total solid angle subtended by the accessible part of the torus by an observer with the line of sight $\hat{\mathbf{k}}_{\mathbf{o}}$ with respect to the light source at the origin is given by

$$\Delta\Omega = \int_{z \ge \frac{h}{2} + 2a \cot \theta_0 \cos \phi} dz \ d\phi \ \frac{a^2}{[a^2 + z^2]^{3/2}}$$

$$= 4 \cot \theta_0 \int_0^{\pi/2} du \ u \sin u$$

$$\times \left[1 + \left(\frac{h}{2a} - 2 \cot \theta_0 \cos u \right)^2 \right]^{-3/2}.$$
(2.14)

Here, we take the cylinder axis as z-axis and $\theta_0 \equiv \cos^{-1} \hat{\mathbf{k}}_{\mathbf{o}} \cdot \hat{\mathbf{z}}$ is the angle between the line of sight and z-axis. In Fig. 2a, a schematic geometry is shown and the hatched region marked by 'A' is the accessible part by the observer.

For parameters h/2a = 1 and $\theta_0 = \cos^{-1} 0.5$, a simple numerical integration of Eq. (2.14) gives the solid angle $\Delta\Omega/4\pi = 0.08$. Hence, this particular geometry mimics a neutral cloud located at high latitude to the observer with the covering fraction ~ 10 percent. However, a tapered disk model investigated by Efstathiou et al. (1995) would give much smaller solid angle. Therefore, only after a detailed geometry of the cicumnuclear region is specified with the appropriate photoionization computation, the covering fraction of the neutral scatterers may be assessed. In this paper we choose a very simple geometry as depicted in Fig. 2b to find the main features of Raman scattering by neutral hydrogen without invoking many free parameters necessary to specify a detailed geometry. In this geometry, the position angle of the polarized radition is perpendicular to the symmetry axis, which is regarded as the radio axis of the active nucleus.

As shown in Fig. 2b, the light source is located at the center and blocked by an opaque component lying equatorially, and the neutral hydrogen component lies alogn z-axis that is coincident with the normal direction of the accretion disk. The geometry of the scatterer is assumed to be an

oblate spheroid with the minor axis aligned to the z-axis. Along the major axes the column density is assumed to be $2N_{H\,\text{I}}$ and inside the scattering region, the number density is assumed to be fixed, which enables us to measure the physical distance in terms of column density. The covering factor C_N of the neutral scatterers is set to be 0.15.

We prepare the UV incident continuum in accordance with the double power law given by Eq. (2.7). We also prepare the line photons around 1030 Å corresponding to the blended Ly β and O VI. We combine the three gaussians centered at 1025 Å, 1032 Å and 1038 Å with the same width of 3000 km s⁻¹ and strength ratio of 1:1.5:1.5. The total blended line flux is renormalized so that it has an equivalent width of 30 Å (e.g. Korista et al. 1997). The possibility for intrinsic anisotropy in the radiation field in the BELR has been suggested and observational evidence is presented for NGC 1068 (Miller et al. 1991, Hough and Young 1995). However for simplicity it is assumed that the light source is isotropic.

As a UV photon reaches the scattering region, it may be first Rayleigh-scattered several times before it is Raman-scattered. It is assumed that the continuum opacity near ${\rm H}\alpha$ is negligible and therefore any Raman-scattered photon leaves the scattering region. Here, the thermal motion of the scatterers is not important because the bulk velocity of the BELR is much larger.

The polarization of the line photon resonantly scattered by a hydrogen atom is dependent on the incident wavelength in the rest frame of the scatterer. However, most UV photons are scattered in the damping wing regime where the deviation from the resonance transition frequency is sufficiently large to ensure that the scattering is characterized by the classical Rayleigh phase function. This is a direct consequence that the fine structure splittings in the np states are negligible compared with the frequency deviation corresponding to the damping wing regime (e.g. Stenflo 1980). Because the final states for both the Rayleigh scattering and the Raman scattering are s states, the same Rayleigh phase function is used to obtain the wave vector and the polarization associated with the scattered photon for both the Rayleigh and the Raman scatterings.

3 RESULTS

3.1 Continuum and Basic Properties

In Fig. 3, we show the scattered flux, the polarized flux and the linear degree of polarization around H α resulting from Raman scattering by neutral hydrogen of column densities in the range $N_{H\,\rm I}=10^{21-22.5}~{\rm cm}^{-2}$. The UV incident spectrum consists of only the continuum given by Eq. (2.7), and we collect the photons with wave vector $\hat{\bf k}$ satisfying $0.45<\hat{\bf k}\cdot\hat{\bf z}<0.55$, where z-axis is the symmetry axis of the AGN.

The polarized flux appears to be a normal $H\alpha$ line with

$$FWHM \sim 1.6 \times 10^4 \ (N_{H \, \text{I}}/10^{22} \ \text{cm}^{-2})^{1/2} \ \text{km s}^{-1}.$$
 (3.1)

This corresponds to a few times the width shown in Eq. (2.4). The scattered flux shows a peak at the line center, and has a red excess that becomes more conspicuous as the column density increases. The polarized flux is broader than the scattered flux and shows a red-shifted

6 Lee and Yun

Figure 2a.

A schematic diagram for a cylindrical molecular torus (see Pier & Krolik 1992). The inner radius is a and the height is h. z-axis is chosen to coincide with the symmetry axis and the central continuum source is located at the origin. The hatched region marked by 'A' can be accessible by the observer with the line of sight $\hat{\mathbf{k}}_0$. Assuming the the observer is in the x-z plane, the region 'A' is described by the relation $z \ge \frac{h}{2a} + 2a \cot \theta_0 \cos \phi$, where $\theta_0 = \cos^{-1} \hat{\mathbf{k}}_0 \cdot \hat{\mathbf{z}}$.

Figure 2b.

A schematic diagram for the scattering model. The continuum light source lies in the center and the broad line photons are generated in the vicinity of the continuum source. The neutral hydrogen component is located along the z-axis, which is coincident with the normal direction to the accretion disk.

Figure 3.

The scattered flux, the polarized flux and the linear degree of polarization around H α Raman-scattered by a neutral hydrogen scattering component of column densities $N_{H\,I}=10^{21},\ 10^{21.5},\ 10^{22},\ 10^{22.5}\ {\rm cm^{-2}}$. The UV incident spectrum is the continuum given by Eq. (2.7), the photons with wave vector $\hat{\bf k}$ satisfying $0.45<\hat{\bf k}\cdot\hat{\bf z}<0.55$ are collected, where z axis is the symmetry axis of the AGN. The solid line represents the scattered flux the dotted line stands for the polarized flux multiplied by 6 for comparison with the scattered flux and the dotted line with error bars for the degree of polarization. The error bars are 1- σ obtained from the Monte Carlo computation.

peaks. The locations of the peak of the polarized flux are given by $\Delta V_{peak} \sim 5600~\rm km~s^{-1}$ for $N_{H\,\rm I}=10^{22.5}~\rm cm^{-2},$ and $\Delta V_{peak} \sim 1700~\rm km~s^{-1},$ and $\sim 800~\rm km~s^{-1}$ for $N_{H\,\rm I}=10^{22}~\rm cm^{-2}$ and $10^{21.5}~\rm km~s^{-1},$ respectively.

Near the line center, the scattering optical depth is very large, and therefore a large scattering number is needed to escape from the scattering region. As the scattering number gets larger, the conversion from Ly β to H α becomes more efficient, and hence we obtain a stronger Raman flux.

Furthermore, the conversion efficiency is dependent on the ratio of the Raman scattering cross section to that of the total scattering cross section in a highly sensitive way. Therefore, as the column density becomes large, the mean scattering number also increases and the strength of the Raman scattered flux is enhanced preferentially to the red part where the ratio of the Raman scattering cross section is larger as shown in Fig. 1.

An illustrative explanation is given by Lee & Lee (1997 b) in their analysis of the Raman scattered flux in symbiotic stars. It is notable that the red asymmetric polarized profile in the high column case is originated from the atomic physics rather than extrinsic factors such as kinematics.

On the other hand, the largest linear degree of polarization is usually obtained when the mean scattering number is ~ 1 , because a large number of scatterings randomize the radiation field associated with the scattered photons and no scattering yields any polarization. However, in the case of the Raman scattering, where the scattered photons are not mixed with the unscattered flux due to the incoherence, the degree of polarization monotonically decreases as the

mean scattering number increases. Therefore, the polarization tends to decrease as the total scattering cross section increases.

Fig. 3 shows that irrespective of the column density, the degree of polarization is the smallest at the H α center, where the total scattering cross section is the largest. It is also interesting that the minimum degree of polarization at the center is approximately constant independent of the scattering column density. This behavior is explained by noting that the Raman flux is mainly contributed from the first few scatterings and that negligibly polarized Raman photons contribute little because of low probability of surviving a large number of Rayleigh scatterings. Near the center, the total scattering optical depth is large enough even for $N_{H\,\rm I}=10^{21}~{\rm cm}^{-2}$ that the polarized flux and the degree of polarization become saturated.

Because the total scattering optical depth rapidly decreases as the wavelength deviation from the center wavelength gets larger, the scattered flux becomes negligible. This is also illustrated by the large error bars in the figure. It is interesting to note that the polarized flux, the total scattered flux and the linear degree of polarization are dependent on the wavelength and the column density of the scatterer, as may be manifested by fine structures in the spectropolarimetric observations.

3.2 Line Contribution and Electron Scattering

In Fig. 4 are shown the same quantities as in Fig. 3 except for the UV incident radiation that includes the line

Figure 4.

The same quantities as in Fig. 3 except for the UV incident radiation includes the line contribution from the Ly β and OVI doublet.

contribution from the Ly β and O VI doublet. A gaussian profile for each line is assumed. With a continuum flux F_c and a line flux

$$F_l = F_0 \exp\left[-(\lambda - \lambda_0)^2 / 2\sigma_l^2\right] \tag{3.2}$$

the equivalent width EW is given by $EW = \sqrt{\pi}\sigma_l(F_0/F_C)$. We take $\sigma_l = \lambda_0(3000~{\rm km~s^{-1}}/c)$ for each line. The equivalent widths of the components of the blended feature are given by $EW_{Ly\beta} = 7.5~{\rm \AA},~EW_{O~VI} = 22.5~{\rm \AA},$ where the doublet O VI is assumed to be contributed equally from $\lambda 1032$ and $\lambda 1038$ components.

The qualitative features shown in Fig. 4 are similar to those in Fig. 3. The main difference is the strength of the polarized flux, due to the increase of the incident UV photons by a factor of \sim 2. Because the Raman-scattering mirror has a narrow band width, the overall variation of the incident UV flux over this mirror-width is small and therefore we obtain qualitatively similar polarized fluxes.

However, because the blended line feature is centered near 1030 Å, the red side of Ly β is stronger than the blue side by a small amount. This leads to more red-asymmetric Raman-scattered flux, which is barely apparent in the figure. The small effect of O VI is due to the small scattering cross section, and the major contribution to the polarized flux is provided by the Ly β line photons which possess a large scattering cross section. When $N_{H\,\rm I} \lesssim 10^{21}~{\rm cm}^{-2}$, the Raman scattering is not important and the asymmetry in the profile is negligible.

In Fig. 5 we compare the Raman-scattered polarized flux with the polarized flux scattered by an electron plasma located in the same position with the same covering factor as the neutral hydrogen scatterer. The column density N_e of the free electron is assumed to be $N_e = 10^{22}$ cm⁻². The incident flux consists of the continuum described in

Eq. (2.7) and the broad H α given by a gaussian with $\sigma_l = 3000 \text{ km s}^{-1}$ and the equivalent width $EW_{H\alpha} = 100 \text{ Å}$.

If we assume that the thermal velocity of the electron plasma is much smaller than the width of the broad $\mathrm{Ly}\beta$, then the line broadening by thermal electrons is neglected. If the Thomson scattering optical depth is also small, then the Thomson scattered flux is mainly contributed from singly scattered photons. Under these assumptions, the electron-scattered flux is characterized by a constant degree of polarization and therefore, the polarized flux has almost the same shape as the that of the scattered flux

Therefore, in this optically thin limit, the degree of polarization p_{Th} of the Thomson scattered flux is given by

$$p_{Th} = \frac{1}{2\pi(1-\mu_e)} \int_{\mu_e}^{1} \int_{0}^{2\pi} d\mu \ d\phi \ \frac{p_1 - p_2}{p_1 + p_2}$$
 (3.3)

where $p_1 = (\cos \theta_o \sin \phi)^2 + (\cos \theta_o \cos \theta \cos \phi + \sin \theta_o \sin \theta)^2$ and $p_2 = \cos^2 \phi + \cos^2 \theta \sin^2 \phi$ are the scattered components that are polarized parallelly and perpendicularly to the plane spanned by the observer's line of sight and the symmetry axis (z-axis) of the system, respectively (e.g. Brown & McLean 1977). Here, θ_o is the angle between the z axis and the observer's line of sight, μ_e is the cosine of the half-angle of the conical region which the electron plasma subtends with respect to the source.

For $\theta_o = \cos^{-1} 0.5$ and $\mu_e = 0.7$, a simple numerical integration gives $p_{Th} = 0.39$, which agrees well with the largest degree of polarization obtained for the Raman scattered flux shown in Fig. 3.

The electron-scattered flux around $H\alpha$ is comparable with the Raman scattered flux for $N_{H\,\rm I}=10^{21.5}~{\rm cm}^{-2}$. We include an unpolarized continuum of strength $\Phi_{uc}=5\times 10^{-3}\Phi_{\lambda}$ as suggested by Tran (1995 c) to compute the

synthetic linear degree of polarization represented by the long-dashed line in Fig. 5. With the polarization-diluting continuum, the degree of polarization shows a bump-like feature around ${\rm H}\alpha$, observed in a number of Seyfert 2 galaxies (e.g. Tran 1995 a,b,c). It is particularly noted that the polarization bumps also have a dip in the center which is ascribed to the decrease of polarization arising from a large number of Rayleigh-Raman scatterings.

4 OBSERVATIONAL IMPLICATIONS

As mentioned in section 2.2, the Raman-scattering material may be regarded as a scattering-mirror with a very narrow band width centered at the resonance frequencies and furthermore the band width provides a natural measure of the column density of the neutral hydrogen. Therefore, when the incident flat continuum is reflected by the Raman-scattering mirror, the scattered continuum appears a line-like feature around the transition frequency $\nu_i - \nu_{Ly\alpha}$.

Stark et al. (1992) presented a H I survey of our galaxy using a beam with a size of FWHM= 2° and showed that the H I column density toward the galactic center amounts to 10^{22} cm⁻². Gallimore et al. (1997) presented the H I column density toward the radio jet of Mrk 6, and showed that neutral hydrogen of column $\sim 10^{21}$ cm⁻² is present around the active nucleus. X-ray observations of many AGN reveal that X-ray absorbing material of $N \sim 10^{20-23}$ cm⁻² around the nuclear region and the physical nature, the exact location and kinematics are currently being investigated intensively.

Ogle et al. (1997) performed a spectropolarimetry of the narrow line radio galaxy Cyg A and found that the full width at half maximum of the polarized H α flux is 26000 km s⁻¹. They noted that the broad emission lines of some radio loud active galaxies show a large velocity width up to 30000 km s⁻¹ with double-peaked profiles (e.g. Eracleous & Halpern 1994). However, Antonucci et al. (1994) observed the same object and measured the width of the broad emission line Mg II \sim 7500 km s⁻¹, which is 3.5 times smaller than that of the polarized H α .

The thermal width of an electron plasma with the temperature T_e is given by

$$v_{th}^e \sim 400 \ T_{e4}^{1/2} \ \mathrm{km \ s^{-1}},$$
 (4.1)

where $T_{e4} = T_e/(10^4 \text{ K})$. If the width of the H α in the polarized flux is interpreted to be caused by hot electrons, then the temperature of the electron plasma $T_e \sim 5 \times 10^7 \text{ K}$ (e.g. Weymann 1970). And there may also exist other polarized lines with a similar width, and it is difficult to explain the width of Mg II line observed by Antonucci et al. (1994).

On the other hand, if the Raman-scattering processes by the neutral component operate, then it may provide an interesting interpretation, i.e., the large width may not be associated with the Doppler effect but mainly an effect of the atomic physics associated with the Raman scattering.

Conway & Blanco (1995) measured the column density of H I toward the compact radio nucleus of Cyg A and obtained a value $\geq 2.54 \pm 0.44 \times 10^{19}~T_s~{\rm cm}^{-2}$, where the spin temperature T_s may go up as high as $1000-8000~{\rm K}$ depending on the physical state of the putative molecular torus obscuring the compact nucleus. Therefore the existence of a high column neutral hydrogen with $N_{H\,I} \gtrsim 10^{22}~{\rm cm}^{-2}$ is not

ruled out. The Raman-scattering by this component may introduce a broad polarized flux with width $\sim 2\times 10^4~\rm km~s^{-1}$ redshifted by $\sim 2000~\rm km~s^{-1}$ from incident UV radiation around Ly β with width $\geq 3000~\rm km~s^{-1}$. Therefore, if we take the width of Mg II 2800 as a representative velocity scale of the BELR, then the spectropolarimetry of Cyg A by Ogle et al. (1997) is consistent with this interpretation.

Young et al. (1993) presented their spectropolarimetric observation of the Seyfert 2 galaxy IRAS 110548-1131 (see also Young et al. 1994). They found a very broad H α line in the polarized flux with a full width at zero intensity of 16800 km s⁻¹ and FWHM= 7600 km s⁻¹, which, they note, is wider than that of most Seyfert 1 galaxies. Another interesting point is that the peak of the broad polarized H α is red-shifted by 900 \pm 400 km s⁻¹ with respect to the narrow H α emission, which they ascribe to an outflow of the scatterers.

If we apply our result, the most plausible column density for IRAS 110548-1131 is $\sim 10^{21.5}~\rm cm^{-2}$, which gives the FWHM of the polarized flux $\sim 10^4~\rm km~s^{-1}$ and the redshift of the peak $\sim 800~\rm km~s^{-1}$.

However, there are other factors that may possibly affect the redshift of the polarized flux. For example, the broad lines are usually redshifted with respect to the narrow emission lines in many AGNs. The amount of redshift differs for various lines, and this may be associated with the stratified structures of the BELR consistent with the reverberation studies of several Seyfert galaxies (e.g. Peterson 1993). In addition to the velocity shift in the source part, the kinematics of the scattering agents is important to determine the overall profile of the scattered (and polarized) flux. In particular, Conway and Blanco (1995) pointed out that the H I component in Cyg A is moving with a typical velocity of several hundred km s⁻¹. We omit the quantitative analysis of this effect in this paper.

The modelling by Young et al. (1996) indicates that the broad lines of IRAS 110548-1131 are polarized by the same degree as the continuum, for which case the Raman scattering is not required. Therefore, if the Raman scattering also operates, then the Raman scattering features may be found only in the fine structures in the polarized flux with high resolution and good signal to noise ratio requiring large amount of integration time.

Here, one example of the fine structures in the polarized flux can be a relative shift of the narrow line peak and that of the polarized flux. The electron-scattered flux reduces the asymmetry in the total scattered flux if the broad ${\rm H}\alpha$ is symmetric. Therefore the relative strength of the electron (and/or dust)-scattered flux affects the location of the polarized flux peak.

Another possible solution may be provided by observing metal lines including Mg II 2800 in the spectropolarimetry mode. Because metal lines have negligible scattering cross section, they will not be scattered by atomic hydrogen and may possess the polarized flux entirely due to free electron. Therefore, the Raman scattered Balmer lines can be shown by verifying different shapes and widths of the polarized fluxes compared with those of metal lines.

One important process expected from a high column neutral hydrogen is the Rayleigh scattering of the photons around the Lyman series lines. The Rayleigh scattering of Ly α photons has been discussed in symbiotic stars by Isliker

et al. (1989). Because the Rayleigh scattering cross section is in general larger than the Raman scattering cross section, it is expected that the Lyman lines are almost as strongly polarized as the Balmer lines.

In this respect, an interesting observation is the HST spectropolarimetry on the quasar PG 1630+337 by Koratkar et al. (1995), who found out a strong polarized flux around Ly α . It is a theoretical possibility that this feature is formed by the Rayleigh scattering process, in which case a more weakly polarized Ly β flux is expected. Because the strong broad line N V 1240 is present at $\sim 6000~{\rm km~s}^{-1}$ to the red side of Ly α , the possibility that the polarized flux is mainly contributed from receding N V is not excluded as noted by Koratkar et al. (1995) (see also Arav et al. 1995).

Therefore UV spectropolarimetry on nearby AGN and optical spectropolarimetry of high redshift AGN will provide strong constraints on the importance of neutral hydrogen scatterings.

5 SUMMARY

We performed a Monte Carlo computation of the linear polarization expected from the Raman scattering process by a neutral hydrogen component in active galactic nuclei. The main features of the Raman scattering processes in AGN include a large width due to the enhancement of the Doppler shift, and a possible red asymmetric polarized flux around ${\rm H}\alpha$ ascribed to the asymmetric conversion efficiency with a smaller contribution of ${\rm Ly}\beta$ and O VI blended broad emission lines.

It is not still clear whether the neutral component with a high column density exists in a typical AGN, and remains a very intersting possibility that the Raman scattering processes provide a natural interpretation of several spectropolarimetric observations of narrow line AGN including Cyg A and IRAS 110548-1131. It is concluded that more detailed comparisons of polarized flux of other metal lines and hydrogen Balmer lines will put stronger constraints on the possible effects of high column neutral components in AGN.

ACKNOWLEDGMENTS

HWL thanks Ki-Tae Kim for providing the information on the H I distribution of our galaxy and external galaxies. He is also grateful to Sang-Hyeon Ahn for helpful discussions about AGN models. JHY wants to express his gratitude to Chan Park for kind advice on fortran programming. We thank the anonymous referee for many useful and important comments which improved this paper.

REFERENCES

Antonucci, R., 1993, ARA&A, 31, 473

Antonucci, R., Hurt, T., & Kinney, A., 1994, Nature, 371, 313 Antonucci, R., Miller, J. S., 1985, ApJ, 297, 621

Arav, N, Korista, K. T., Barlow, T. A., Begelman, M. C., 1995, Nature, 376, 576

Bethe, H. A. & Salpeter, E. E., 1967, Quantum Mechanics of One and Two Electron Atoms, Academic Press Inc., New York

Berestetskii, V.B., Lifshitz, E.M., & Pitaevskii, L.P., 1972, Relativistic Quantum Mechanics Pergamon Press Inc., New York Brown, J. C. & McLean, I. S., 1977, A&A, 57, 141

Cohen, M. H., Ogle, P. M., Tran, H. D., Vermeulen, R. C., Miller,
J. S., Goodrich, R. W., & Martel, A. R., 1995, ApJ, 448, L77
Conway, J. E., & Blanco, P. R., 1995, ApJ, 449, L131

Dickey, J. M., 1986, ApJ, 300, 190

Efstathiou, A., Hough, J. H., & Young, S., 1995, MNRAS, 277, 1134

Eracleous, M. & Halpern, J. P. 1994, ApJS, 90, 1

Gallimore, J. F., Baum, S. A., O'Dea, C. P., Brinks, E., Pedlar, A., 1994, ApJ, 422, 13

Gallimore, J. F., Holloway, A. J., Pedlar, A., Mundell C. G., 1998, A&A, 333, 13

Gavrila, M., 1967, Phys. Rev., 163, 147

Goodrich, R.W., Miller, J. S., 1995, ApJ, 448, L73

 $Hough,\,J.\,\,H.\,\,\&\,\,Young,\,S.,\,1995,\,MNRAS,\,277,\,1134$

Isliker, H., Nussbaumer, H., & Vogel, M., 1989, A&A, 219, 271

Koratkar, A., Antonucci, R. R. J., Goodrich, R. W., Bushouse, H., Kinney, A. L., 1995, ApJ, 450, 501

Korista, K., Baldwin, J., Ferland, G., & Verner, D., 1997, ApJS, 108, 401

Koski, A.T., 1978, ApJ, 223, 56

Kriss, G.A., Davidsen, A.F., Zehng, W., Kruk, J.W., & Espey, B.R., 1995, ApJ, 454, L7

Laor, A, Bahcall, J. N., Jannuzi, B. T., Schneider, D. P., Green, R. F., 1995, ApJS, 99, 1

Laor, A, Bahcall, J. N., Jannuzi, B. T., Schneider, D. P., Green, R. F., Hartig, G. F., 1994, ApJ, 420, 110

Lee, H.-W., & Blandford, R. D, 1997, MNRAS, 288, 19

Lee, H.-W., & Lee, K. W., 1997a, MNRAS, 287, 211

Lee, K. W., & Lee, H.-W., 1997b, MNRAS, 292, 573

Mathews, W.G., Ferland, G.J., 1987, ApJ, 323, 456

Miller, J. S., & Goodrich, R. W., 1990, ApJ, 355, 456

Miller, J. S., Goodrich, R. W. & Mathews, M. G., 1991, ApJ, 378, 47

Mundell, C. G., Pedlar, A., Baum, S. A., O'Dea, C. P., Gallimore, J. F., Brinks, E., 1995, MNRAS, 272, 355

Nandra, K., George, I. M., 1994, MNRAS, 267, 974

Natali, F., Giallongo, E., Cristiani, S., & La Franca, F., 1998 AJ, 115, 397

Netzer, H. 1990, Active Galactic Nuclei, Springer-Verlag

Netzer, H., 1993, ApJ, 411, 594

Nussbaumer, H., Schmid, H. M.& Vogel, M., 1989, A&A, 221, L27
Ogle, P.M., Cohen, M. H., Miller, J. S., Tran, H. D., Fosbury, R. A. E. & Goodrich, R. W., 1997, ApJ, 482, L37

Osterbrock, D. E., 1989, Astrophysics of Gaseous Nebulae abd Active Galactic Nuclei, University Science Books, Mill Valley Peterson, B. M., 1993, PASP, 105, 247

Pier, E. & Krolik, J., 1992, ApJ, 401, 99

Saslow, W. M., & Mills, D. L., 1969, Phys. Rev., 187, 1025

Sadeghpour, H. R. & Dalgarno, A., 1992, J. Phys. B: At. Mol. Opt. Phys., 25, 4801

Sakurai, J. J., 1967, Advanced Quantum Mechanics Addison-Weseley Publishing Company. Reading, Massachusetts

Schmid, H. M., 1989, A&A, 211, L31

Stark, A. A., Gammie, C. F., Wilson, R. W., Bally, J., Linke, R. A., Heiles, C., Hurwitz, M., 1992, ApJS, 79, 77

Stenflo, J. O. 1980, A&A, 84, 68

Tran, H. D., 1995a, ApJ, 440, 565

Tran, H. D., 1995a, ApJ, 440, 578

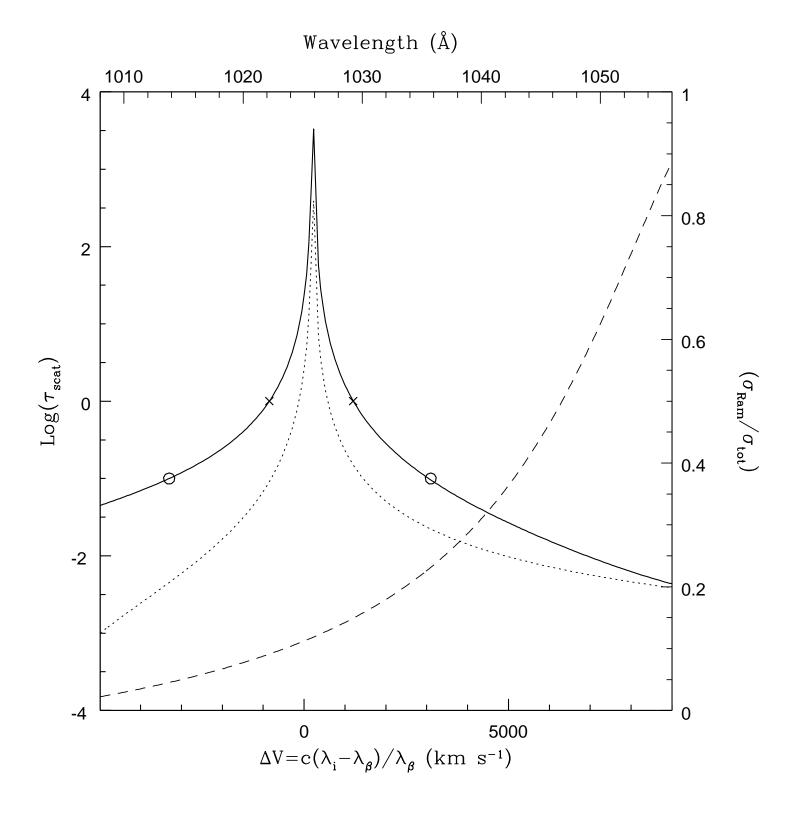
Tran, H. D., 1995a, ApJ, 440, 597

Turner, T.J., Netzer, H., & George, I. M., 1996, ApJ, 463, 134
Ueno, S., Koyama, K., Nishida, M., Yamauchi, S. & Ward, M.J., 1994, ApJ, 431, L1

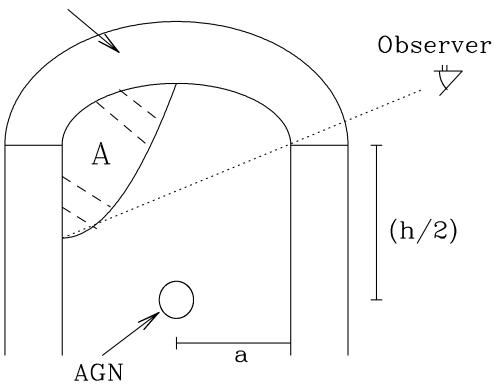
Weymann, R., 1970, ApJ, 160, 31

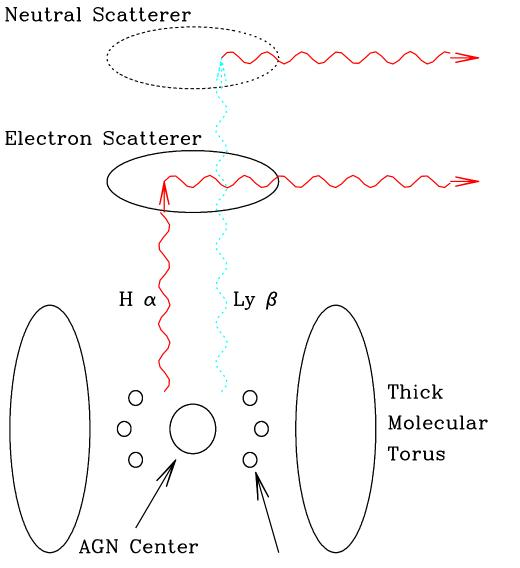
Young, S., Hough, J. H., Bailey, J. A., & Axon, D. J., 1994, The Nature of Compact Objects in Active Galactic Nuclei, ed. A. Robinson and R. Terlevich, Cambridge University Press, Cambridge Young, S. Hough, J. H., Efstathiou, A., Wills, B. J., Bailey, J. A., Ward, M. J., & Axon, D. J., 1996, MNRAS, 281, 1206
Young, S., Hough, J. H., Bailey, J. A., Axon, D. J.& Ward, M. J., 1993, MNRAS, 260, L1
Zheng, W., Kriss, G. A., Telfer, R. C., Grimes, J. P., & Davidsen, A. F., 1997, ApJ, 475, 469

This paper has been produced using the Royal Astronomical Society/Blackwell Science TEX macros.



Molecular Torus





Broad Emission Line Region

